*Journal of Structural Geology*, Vol. 11, No. 4, pp. 407 to 419, 1989
Printed in Great Britain

0191-8141/89 $03.00 + 0.00


# Alleghanian tectono-thermal evolution of the dextral transcurrent Hylas zone, Virginia Piedmont, U.S.A.

ALEXANDER E. GATES

Department of Geology, Rutgers University, Newark, NJ 07102, U.S.A.

and

LYNN GLOVER, III

Orogenic Studies Laboratory, Department of Geological Sciences, Virginia Polytechnic Institute and State University, Blacksburg, VA 24061, U.S.A.

(*Received* 19 *July* 1988; *accepted in revised form* 11 *December* 1988)

**Abstract**—The Hylas zone is the northernmost segment of the Eastern Piedmont fault system and lies in the Grenville Goochland terrane, Virginia. Like the other major segments, the Nutbush Creek zone, the Hollister zone and the Modoc (Irmo) zone, the Hylas zone experienced late Paleozoic dextral transcurrent shearing. Early deformation in the zone was ductile and produced type I and type II *S–C* mylonites under amphibolite-grade metamorphic conditions. Later deformation was at the brittle–ductile transition at which time feldspar underwent microfaulting and cataclasis while quartz formed ribbons. The feldspar exhibits a strain-dependent sequence of microstructures, including kink-bands, antithetic extensional microfaults (pull-apart), bends in the microfaults by development of transverse fractures and microboudinage. Correlation of mineral mechanical response with a thermal-decay curve based on isotopic mineral ages yields a temporally constrained deformation history. Ductile dextral shearing occurred subsequent to the intrusion of the 330 Ma Petersburg granite and passed into the brittle–ductile transition by approximately 260 Ma. Dextral faulting terminated before 240 Ma. The Appalachian dextral transcurrent faulting event therefore continued through Permian in some areas.

## INTRODUCTION

THE Hylas mylonite zone (Bobyarchick & Glover 1979) is the northernmost segment of the Eastern Piedmont fault system in the southern Appalachian Piedmont (Fig. 1) (Hatcher *et al.* 1977). The other major segments, the Nutbush Creek zone (Bartley *et al.* 1984, Druhan & Rollins 1984), the Hollister zone (Smits *et al.* 1988) and the Modoc (Irmo) zone (Secor *et al.* 1986, Dennis & Secor 1987), had late Paleozoic dextral transcurrent movement (first proposed by Bobyarchick 1981). Movement on the Nutbush creek zone is constrained to between 313 ± 15 Ma and 285 ± 10 Ma by the intrusion of the pre- to syn-kinematic Buggs Island and post-kinematic Wilton granitic plutons into the zone (Druhan & Rollins 1984). The 292 Ma Butterwood Creek Pluton is syn-kinematic with respect to the Hollister zone and movement on the Modoc (Irmo) zone is constrained to between 285 and 267 Ma as a result of detailed $^{40}Ar$–$^{39}Ar$ dating of minerals in the Kiokee belt (Dallmeyer *et al.* 1986).

This study places the Hylas mylonite zone into context with the rest of the Eastern Piedmont fault system through the documentation of dextral transcurrent movement. Deformation at the brittle–ductile transition produced a strain-related sequence of brittle microstructures in granitic rocks. Mineral deformation is correlated with a thermal-decay curve of the area that is based on $^{40}Ar$–$^{39}Ar$ and fission-track isotopic dating. The correlation yields a constrained deformation history. Timing of Alleghanian dextral transcurrent movement in the Hylas zone has tectonic implications for the entire Eastern Piedmont fault system.

## TECTONO-STRATIGRAPHY

The Hylas zone lies in the Grenville-age Goochland terrane of the eastern Virginia Piedmont (Fig. 2). The tectono-stratigraphy of the area is summarized by Farrar (1984). The stratigraphic sequence is uncertain because no sedimentary facing data exist. The units in the area are the State Farm Gneiss and the Maidens Gneiss and several intrusive units. This classification differs from Farrar (1984) in the elevation of the Maidens Gneiss to group status, including both the previous Maidens Gneiss and the Sabot Amphibolite. There are Triassic–Jurassic diabase dikes and terrestrial siliciclastics in this area that are not considered in detail for this study. Mylonite clasts in the Triassic sedimentary rocks, however, yield a minimum age for ductile deformation.

The tectono-stratigraphy is summarized in Table 1. The Hylas and related shear zones occur in all of the lithologies but are best expressed in granitic gneisses and aluminous gneisses and schists. The State Farm Gneiss is the structurally lowest unit and comprises the cores of several structural domes in the area (Figs. 2 and 3). It consists dominantly of granitic to tonalitic, biotite- and/or hornblende-bearing gneiss (Reilly 1980). Samples of the State Farm granitic gneiss from the type area have been dated at 1031 ± 94 Ma using Rb–Sr whole-rock methods (Glover *et al.* 1978, 1982).

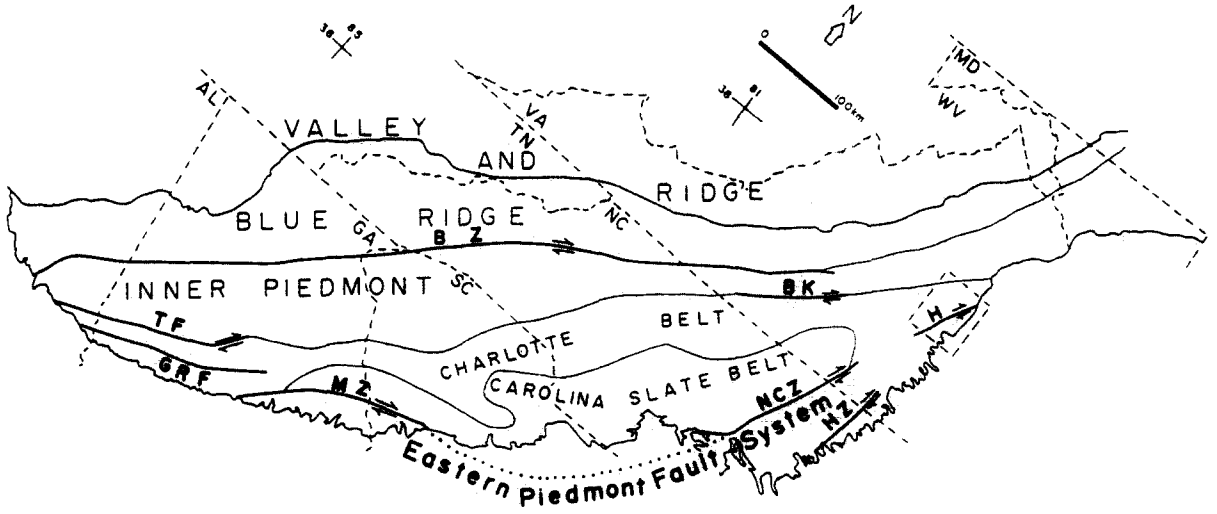


Fig. 1. Tectonic map of the southern Appalachians with major provinces and traces of faults with dextral transcurrent or transpressional deformation (indicated by arrows) including those of the Eastern Piedmont fault system. Outlined area is that shown in Fig. 2. H = Hylas zone, HZ = Hollister zone, NCZ = Nutbush Creek zone, BK = Brookneal zone, MZ = Modoc (Irmo) zone, BZ = Brevard zone, and possible extensions of the Eastern Piedmont fault system, TF = Towaliga fault, GRF = Goat Rock fault (after Glover *et al.* 1983; Gates *et al.* 1986; Williams 1978).

The Maidens Gneiss Group overlies the State Farm Gneiss in gradational to sharp contact (Fig. 2). The lower section of the Maidens Gneiss Group is dominated by amphibolites, including the Sabot Amphibolite, and quartzite, whereas the upper section is dominated by aluminous schist and gneiss and small granite bodies (Fig. 3).

The Petersburg granite (Fig. 2) intruded the Goochland terrane at 30 ± 8 Ma as determined through U–Pb dating of zircons (Wright *et al.* 1975). The Petersburg granite is a fine- to coarse-grained, muscovite–biotite monzogranite that is pre-kinematic with respect to the Hylas zone and strongly deformed within it (Bobyarchick & Glover 1979).

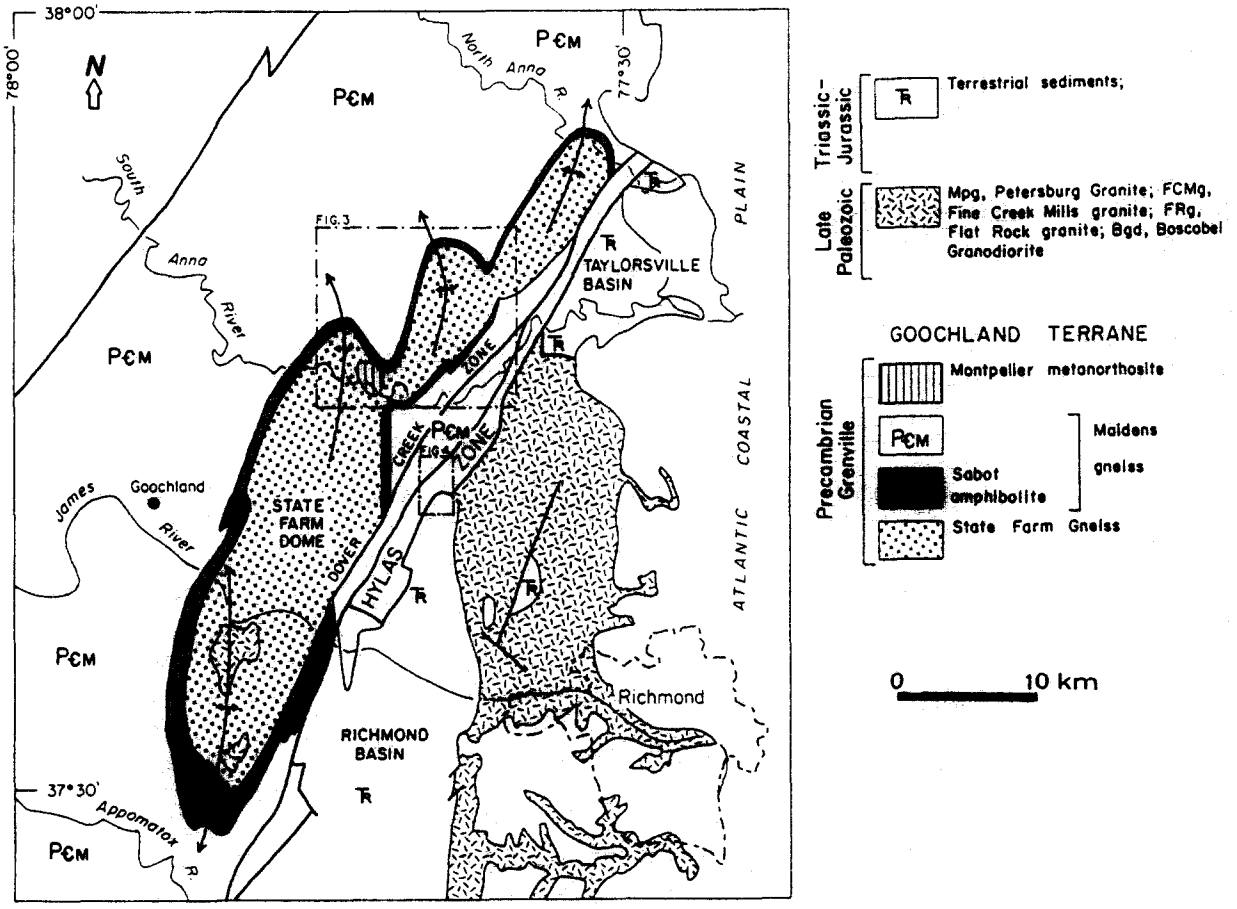


Fig. 2. Geologic map of the Goochland terrane, eastern Piedmont Virginia (modified from Farrar 1984). Faults in heavy lines; arrowed lines are major fold axes. Outlined north area in Fig. 3, south area in Fig. 4.

Table 1. Tectonostratigraphy of the eastern Virginia Piedmont

| | | |
|---|---|---|
| Petersburg Granite | | Medium to coarse grained granite, foliated to mylonitic with K-spar, quartz, plagioclase, biotite, muscovite, apatite, zircon, opaques |
| Montpelier Anorthosite | | Unfoliated, very coarse grained, antiperthitic plagioclase with quartz, apatite, rutile, ilmenite, sphene, diopside, and foliated, medium grained anorthosite with hornblende, biotite and muscovite |
| Maidens Gneiss Group | Granulite (west) | Medium grained, foliated to massive, orthopyroxene, clinopyroxene, plagioclase, garnet, with ilmenite, rutile, quartz, K-spar, hornblende and biotite locally |
| | Granitic Gneiss (east) | Foliated to mylonitic, medium to coarse grained hornblende granitic gneiss with K-spar, plagioclase, quartz, hornblende, garnet, apatite, muscovite and opaques and hornblende-biotite granitic gneiss with biotite and excluding garnet |
| | Quartzite | 95 to 98% quartz with biotite and opaques |
| | Calc-silicate | Scapolite-diopside schist/gneiss with plagioclase, epidote, tremolite, phlogopite, K-spar, clinozoisite, calcite, apatite, opaques |
| | Granite Pods | Foliated to mylonitic, medium grained alkali-feldspar granite to monzogranite with K-spar, quartz, plagioclase, biotite, muscovite, garnet, chlorite, epidote, opaques |
| | Aluminous Gneiss | Biotite-garnet migmatitic gneiss with muscovite, quartz, plagioclase, kyanite, staurolite, K-spar, sillimanite, apatite, rutile, opaques, contains K-spar rich leucosome with quartz, plagioclase, biotite, and kyanite |
| | Sabot and other Amphibolite | Hornblende-andesine schist/gneiss with clinopyroxene cores in hornblende, accessory sphene, apatite, magnetite, ilmenite. Variably layered to massive |
| State Farm Gneiss | | Medium-coarse grained granodiorite to hornblende diorite with plagioclase, quartz, K-spar, bioitite, garnet, hornblende, sphene, apatite, opaques, rutile, appears gradational from the diorite to Sabot amphibolite locally, otherwise contact is sharp. Very coarse grained garnet-biotie gneiss with K-spar, muscovite, quartz and kyanite or sillimanite |

## METAMORPHISM

The metamorphism of the Goochland terrane near the Hylas zone is the product of two distinct events. Farrar (1982, 1984) identified an early granulite facies metamorphism ($M_g$) that affected the State Farm Gneiss and Maidens Gneiss Group. The granulite metamorphism is best represented by two-pyroxene, sillimanite–microcline and orthopyroxene–garnet, granulites of the Maidens Gneiss Group dominantly to the west and northwest of the State Farm and related domes (Figs. 2 and 3) (Farrar 1984). Towards the southeast, these granulite assemblages were largely replaced by amphibolite-facies assemblages of the later $M_1$ retrograde metamorphism. The $M_1$ amphibolite-facies metamorphism produced assemblages dominated by muscovite, garnet, kyanite, fibrolitic sillimanite, staurolite and biotite in the aluminous rocks and hornblende, andesine and diopside in the mafic rocks. Farrar (1984) suggests pressures of 5–7 kb and temperatures of 550–650°C for peak $M_1$ conditions. The relict granulite-facies minerals near the Hylas zone are microcline and granular sillimanite that are mainly replaced by muscovite and kyanite in the aluminous gneisses and ortho- and clinopyroxene replaced by hornblende, biotite and garnet in the mafic rocks.

The $M_g$ granulite-facies metamorphism is proposed to be of Grenville age (Farrar 1984) because the 1031 ± 94 Ma State Farm Gneiss exhibits the same granulite-facies mineral assemblages as those in the overlying Maidens Gneiss Group and the Goochland terrane is similar to the other Grenville provinces in the southern Appalachians. The $M_1$ amphibolite-facies metamorphism overprints the $M_g$ assemblages in the vicinity of the Hylas zone and appears closely related to deformation associated with dextral strike-slip shearing.

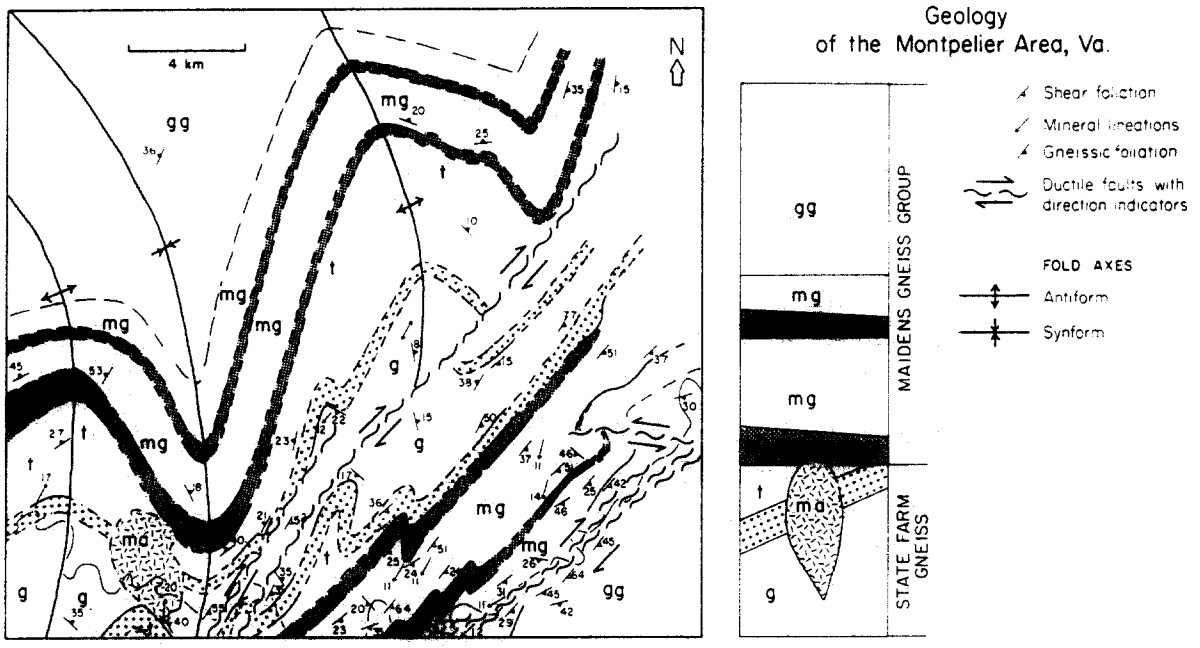


Fig. 3. Geologic map of the Montpelier–Hanover Academy area (based on unpublished map by Gates *et al.* 1987) (location on Fig. 2). State Farm Gneiss includes lower granitic gneiss (g) which is gradational into upper tonalitic gneiss (t), both containing metapelite (crosses). Montpelier Anorthosite (ma) intrudes State Farm Gneiss and possibly the Sabot Amphibolite. Maidens Gneiss Group is combined except for continuous amphibolite layers (heavy shade). Lower amphibolite is Sabot Amphibolite. There are metasedimentary rocks (mg) between the amphibolites. Overlying this sequence are thinly layered metasedimentary rocks (mg) succeeded by granitic and granulite gneiss (gg) (see Table 1).

Aligned amphibole replaces pyroxene, and plagioclase is dynamically recrystallized in sheared metamafic rocks. In the sheared granites and aluminous gneisses of the Maidens Gneiss Group, kyanite is commonly aligned in the mylonitic foliation and garnets exhibit helicitic inclusion trails and rotated biotite-bearing strain shadows. $^{40}Ar$–$^{39}Ar$ mineral dates from the amphibolite-grade rocks yield ages of 262 Ma (hb) and 241 Ma (bt) (Durrant 1979, Durrant *et al.* 1980). The $M_1$ metamorphism is therefore late Paleozoic or older in age and attributed to the Alleghanian event (Durrant *et al.* 1980, Farrar 1982, 1984, Glover *et al.* 1983). Triassic normal faulting reactivated the Hylas zone and associated retrogression produced chlorite, epidote, hematite, zeolites and calcite in the joints and cataclasites.

## EARLY DEFORMATION

There was an intense deformational event ($D_g$) associated with the granulite-facies metamorphism. The $D_g$ event (Farrar 1984) produced a penetrative $S_g$ foliation and recumbent isoclinal, intrafolial $F_g$ folds that are well displayed in the State Farm and Maidens Gneisses. To the west of the domes, the foliation and rock units dip gently westward both in surface outcrop (Bourland 1976, Poland 1976, Reilly 1980) and in subsurface, as shown on seismic reflection profiles (Harris *et al.* 1982, Pratt *et al.* 1988). The Hylas zone and domed area may have exhibited similar gently-dipping, near-homoclinal features prior to Alleghanian deformation. The early $D_g$ and late Triassic extensional events are not considered in detail.

## LATE PALEOZOIC STRUCTURAL FEATURES

The dextral Hylas zone is the most prominent structural feature in the study area. The zone is a 0.5–2.4 km wide, NE-trending band of mylonite that generally dips steeply to the southeast (Bobyarchick & Glover 1979). The Hylas zone proper crosses the Petersburg granite and units of the middle and upper Maidens Gneiss Group. A series of anastomosing ductile shear zone splays that join the Hylas zone, however, cross all units of the Goochland terrane (Fig. 3). The Dover Creek zone (Fig. 2) (Bobyarchick 1976) was considered a separate fault but recent mapping indicates that it joins with the Hylas zone. There are several other NE-trending dextral splays. Shear zones exhibiting deformation at the brittle–ductile transition form thin bands that lie both within and outside of the purely ductile zones. In many cases, the semi-brittle deformation is imposed directly on the ductile features, clearly post-dating them. Otherwise, the intense semi-brittle deformation obliterated earlier textures. The semi-brittle zones are ductile on the bulk scale but exhibit brittle deformation of some minerals both on mesoscopic and microscopic scale. Thin brittle zones are interspersed with the semi-brittle zones and appear to be gradational with them. Minor sinistral transcurrent zones are NW-trending and steeply dipping. The zones are semi-brittle to ductile, antithetic to the dextral zones but late, commonly crossing wider dextral mylonites (Fig. 3).

## MICROSTRUCTURAL KINEMATIC INDICATORS

The microstructural kinematic indicators in the Hylas

zone and small anastomosing shear zones are divided into three groups: those formed in the ductile regime, those formed at the ductile–brittle transition and those formed in the brittle regime. Minerals in rocks that record deformation in the ductile regime exhibit syn-kinematic recrystallization. At the ductile–brittle transition, some minerals exhibit fracture and cataclasis as do all minerals in the brittle regime.

*Ductile strain features*

Shear bands (extensional crenulation cleavage of Platt & Vissers 1980), rotated porphyroclasts and quartz ribbons were formed in the sheared aluminous gneiss of the Maidens Gneiss Group. The shear bands offset migmatite leucosome veins in small step-like extension faults with a consistent dextral transcurrent shear sense. The shear bands are oriented at approximately 19–25° to the shear-zone boundary as determined on map scale. Shear bands are defined by finely recrystallized feldspars, mica and quartz and the porphyroclast edges sweep into them. Biotite and muscovite also form sigmoidal porphyroclasts (mica fish of Eisbacher 1970) that show dextral movement sense. In some areas, kyanite laths are aligned in the shear bands and were locally pulled apart. Rotated garnets exhibit asymmetric mica–quartz strain shadows that define $\delta$-type porphyroclasts (Passchier & Simpson 1986) and rarely contain helicitic inclusion trails. Quartz forms polycrystalline ribbons (type 2B of Boullier & Bouchez 1978) that define the major foliation.

Ductile deformation of the Petersburg granite produced a type I *S–C* mylonite of Lister & Snoke (1984) with rotated mica and feldspar porphyroclasts. The *C* and *S* bands (Berthé *et al.* 1979) demonstrate an unequivocal dextral shear sense (Figs. 4 and 5). The *S* bands are defined by muscovite, biotite and type B2 quartz ribbons (Boullier & Bouchez 1978). The *C* bands are defined by recrystallized mica and strike approximately parallel to the mapped shear-zone boundary. The *S* bands curve asymptotically into the *C* bands, as do $\sigma$-type sigmoidal recrystallized feldspar porphyroclasts (Passchier & Simpson 1986) and mica fish (Eisbacher 1970, Lister & Snoke 1984). Mineral stretching lineations in mylonite plunge approximately 8–20° to the southwest and indicate a reverse component to the transcurrent movement or later folding.

*Brittle–ductile transition features*

Deformation of the Petersburg granite at the brittle–ductile transition was characterized by brittle feldspar and ductile quartz responses. Quartz forms highly strained, sigmoidal-shaped, type B1 polycrystalline ribbons (Boullier & Bouchez 1978) that show subgrain formation and curvature in a consistent dextral sense. The quartz ribbons are intergrown with strained muscovite, biotite and chlorite porphyroclasts or mica fish (Eisbacher 1970). The ribbons and subgrains are oriented at an acute angle to the flow plane ($S_f$–$S_c$ quartz

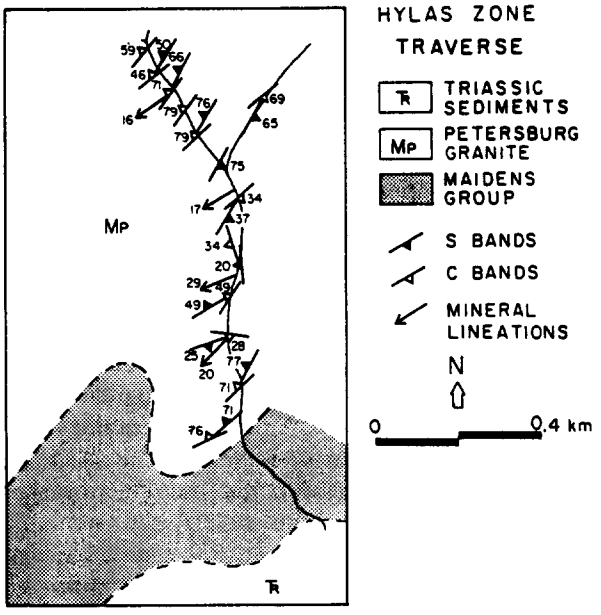


Fig. 4. Geologic map of the southern detailed map area (see Fig. 2) with *C* and *S* bands in Petersburg granite.

ribbons of Simpson 1986) and with the mica form type II *S–C* mylonites (Lister & Snoke 1984). The quartz–mica mylonite formed the matrix within which the brittle feldspars floated.

The feldspars show fracturing and grain-size reduction through cataclasis. Strain cannot be determined accurately from the extension and fragmentation of feldspar grains because of the competency differences between the brittle feldspar and ductile matrix. The grains can be reconstructed, however, through careful analysis of fragments and their displacement. Minimum elongation of the feldspar grains can be calculated (method described in a later section), supplying a semi-quantitative index of deformation for individual grains. The strains are minimum values because fragmentation or chemical reaction that might remove feldspar into the matrix (volume loss) cannot be taken into account.

At lower strain conditions, plagioclase displays kink bands (Fig. 6a) that grade directly into microfaults or small cataclastic bands within the grain. A shortening of 8.7% by kink-banding is calculated for the plagioclase in Fig. 6(a). Strain in K-spar grains may not be comparable. The orientation of kink-bands in feldspar was shown to be crystallographically controlled in another study (Debat *et al.* 1978). The K-spar also displays kink bands but is more commonly pulled apart along extensional microfaults (Fig. 6b). The microfaults follow cleavage planes and movement sense (with respect to the flow) in observed K-spar and plagioclase at higher strain, was consistently antithetic. Parallel cigar- and dovetail-shaped lamellar intergrowths of quartz (analyzed using SEM-EDS) form perpendicular to relatively straight microfaults within the microfault blocks. The intergrowths are concentrated at the microfaults and appear to have been strain induced. Elongation through microfaulting is 26.8% in Fig. 6(b) but may be greater if the quartz intergrowths are extensional features and

increase the volume. Bulbous strain-induced myrmekites (Simpson 1985) occur at K-spar grain boundaries in all strain conditions.

The microfaults were bent into the shear plane at higher strain conditions (Fig. 6c). The bending of the microfault blocks was a brittle process in which sharply defined transverse microfractures formed along the block. Some of the microfractures form zones of microcataclasis. The bending of the microblocks caused lattice misorientation that can be recognized by sweeping extinction along them. The axial plane of bending is oriented at the conjugate angle to the microfaults though the bending clearly post-dates the faulting. The extension is 44.8% in the curving of microfaults in Fig. 6(c).

In the final stage of increased strain, the microfault blocks were bent into the shear plane and the transverse microfractures propagated and coalesced to yield offset of feldspar fragments (Fig. 6d). The fragmented feldspar microfault blocks form boudins that are surrounded by optically continuous quartz. The elongation is 55.2% in Fig. 6(d), the fragmentation stage. The higher strain stages probably had the most submicroscopic cataclastic flow and are subject to the highest errors. The orientation of the grains with respect to the flow plane is relatively constant but the rate at which the grain rotated (vorticity) may have affected the microstructural response.

*Grain reconstruction*

Brittle grains may have deformed in several ways, both in compression or extension depending upon their orientation in the mylonitic flow (Simpson & Schmid 1983, Simpson 1986). In this reconstruction, only extended grains are considered because few compressed grains were observed.

Beginning with the most deformed grain (Fig. 6d), the microboudins of feldspar are reattached to each other and the microfault blocks are reconstructed (Fig. 7a). Each boudin is attached to the neighboring adjacent grain assuming minimal rotation and linear extension. The reconstructed grain contains curved microfaults and blocks like that in Fig. 6(c). The microfaults are then bent into straight lines (planes) (Figs. 6a and 7b). The angle to which the faults are bent is ideally that at the center and least deformed part of the grain. In Figs. 6(c) & (d), however, one side of the grain is far less deformed than the other. The angle of the faults at the least deformed edge served as the reference angle in reconstruction. The area of the grain with the least amount of transverse fractures probably contains the best reference angle because bending is accommodated unequally along these features. The bending of the faults approximately reflects shear strain for that part of the deformation, but because there is some slip along the fault planes during bending, they are not truly passive markers. The bending is also not homogeneous because more bending occurs at the transverse fractures than in other areas.

The final step is the retrodeformation of the extensional faults to reproduce the original grain (Fig. 7c). The reconstruction assumes no rotation of the original grain unless determinable by alternate methods. If there was an original preferred orientation of feldspar that can be identified outside of the shear zone, then rotation can be determined. Elongation can be calculated by comparing total length of undeformed with deformed grains. The more accurate method is to consider each microfault block by calculating the bending and boudinage separately from the retrodeformation of the extensional faults. Shear strain is a more representative quantity for these features because they occur in a shear zone and for the bending and microboudinage stages (Figs. 7a & b) it can be roughly estimated by comparing angles. Assumption of initial angle of the grain however, must be made to evaluate microfaulting (Fig. 7c). Rotation of the grain prior to microfaulting cannot be addressed. Because the strain is not homogeneous across the grain and submicroscopic cataclastic flow (Tullis & Yund 1987) is not considered, all of the calculations are more realistically lower bound estimates.

Total strain may not be the only factor in the development of these textures. All four microstructures (Figs. 6a–d) have been observed in a single grain, each grading into the other in the appropriate order of strain with higher values closer to the mylonitic flow plane. In a few cases, however, the extensional fault, pull-apart textures accommodate as much or more strain than the two 'more deformed' stages. Bending or rotation of the microfault towards parallelism with the flow plane could also potentially record more strain than the microboudinage stage.

The deformation features exhibited by the quartz ribbons, feldspar and micas from the Hylas zone compare with those from the lower to lower middle greenschist facies in the Eastern Penninsular Ranges mylonite zone (Simpson 1985) and North Armorican shear zone (Watts & Williams 1979). The metamorphic assemblage of chlorite, biotite, zoisite and albite associated with deformation, supports greenschist-facies conditions. The bulbous strain related myrmekites are proposed to only be formed in amphibolite-facies conditions (Simpson 1985) and may be vestiges of the earlier high-temperature deformation.

*Brittle features*

Irregularly spaced, 1–2 mm cataclasite layers are interlayered with and have the same orientation as the semi-brittle zones. In these layers, quartz is also fragmented and with feldspar forms a cataclasite with layered to randomly oriented fabric. Where determinable, offset is dextral or sinistral and antithetic. The brittle deformation clearly post-dates the ductile deformation.

*Other structures*

The State Farm dome and related NE-trending, en échelon domes are amalgamated into a major NE-trending antiform that bounds the western margin of the Hylas zone (Fig. 2). Individual domes have NNW–NE-trending fold axes that curve asymptotically into the

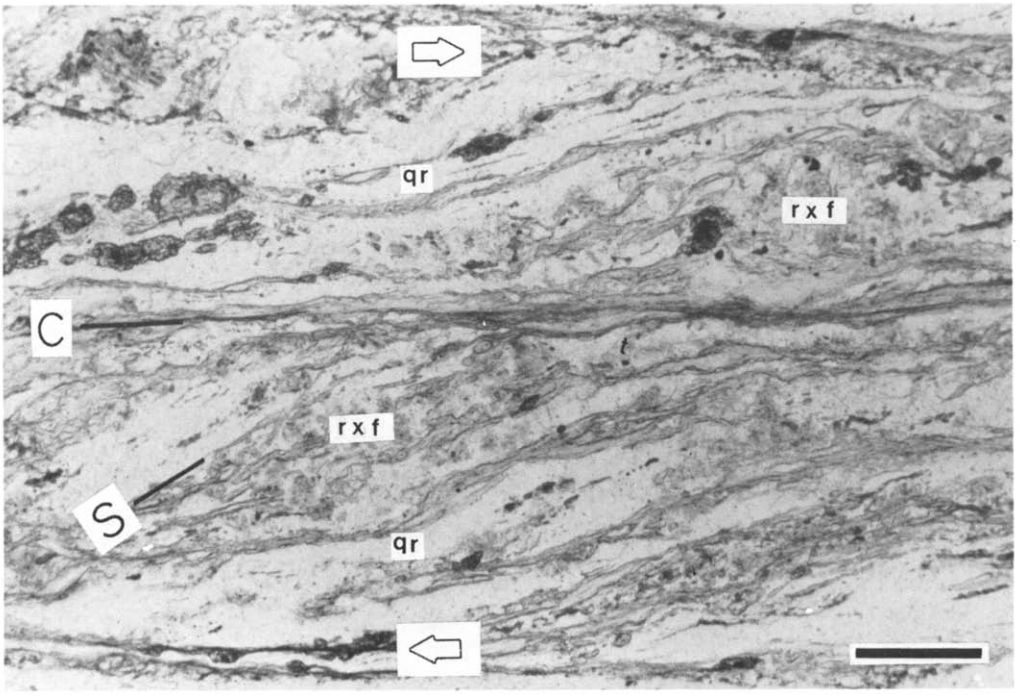


Fig. 5. *C* and *S* bands (Berthé *et al.* 1979) in the Petersburg granite from the Hylas zone proper. Mica folia with rxf = recrystallized feldspar and qr = quartz ribbons. Arrows show relative offset. Scale bar = 0.5 mm.

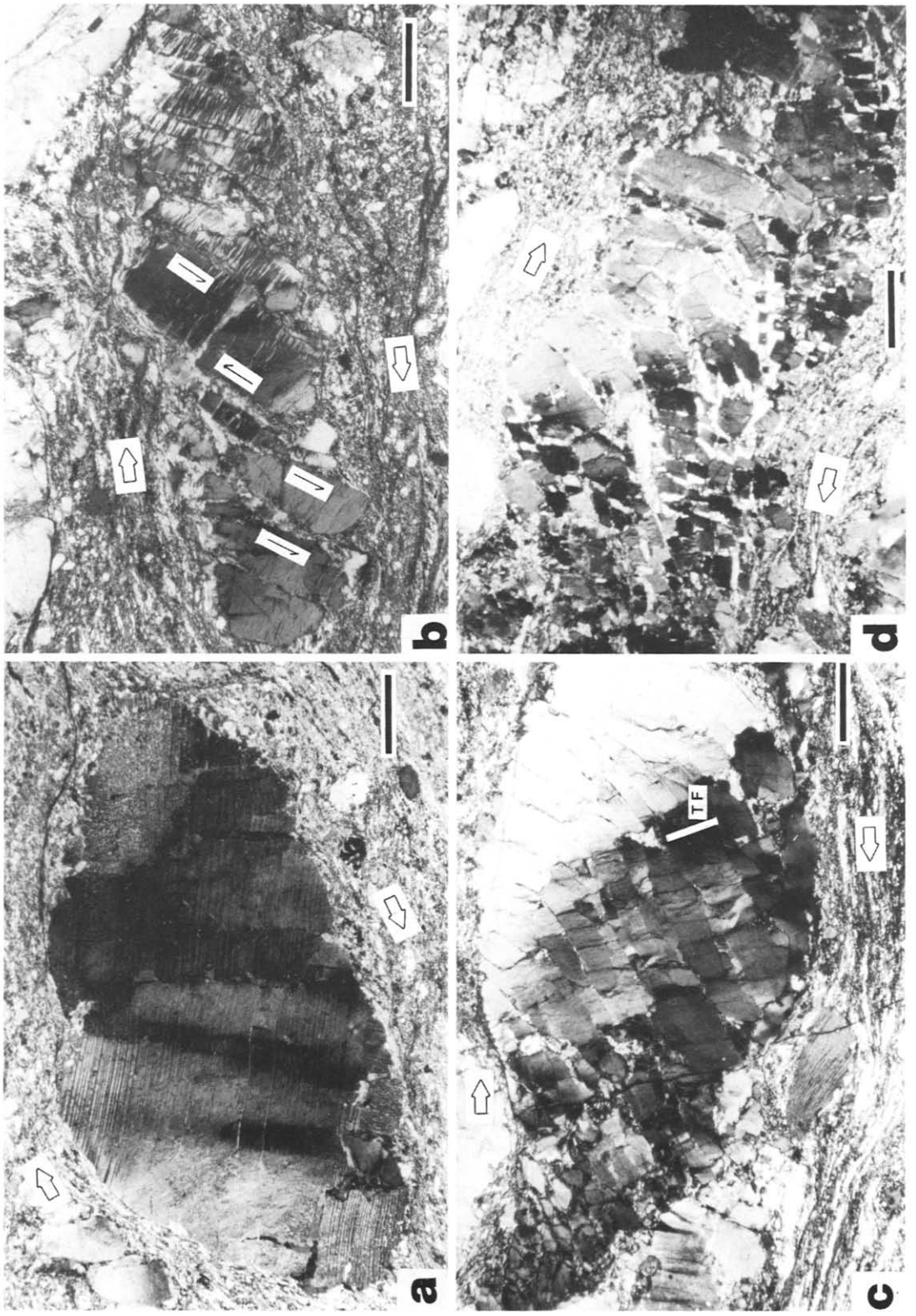


Fig. 6. (a) Kink banding in plagioclase grain in quartz ribbon–mica matrix. Arrows indicate shear direction. Scale bar = 0.5 mm. (b) Relatively straight extensional microfaults in K-spar within quartz ribbon–mica matrix. Lamellar intergrowths are quartz. Small arrows indicate movement on brittle microfaults, large arrows indicate overall movement on shear zone. Scale bar = 0.5 mm. (c) Curved extensional microfaults and transverse microfractures (TF) in K-spar with sweeping extinction. Arrows indicate movement on shear zone. Scale bar = 0.5 mm. (d) Boudinage or fragmentation of microfault blocks, propagation of microfractures and infill with optically continuous quartz. Arrows indicate movement on shear zone. Scale bar = 0.5 mm.

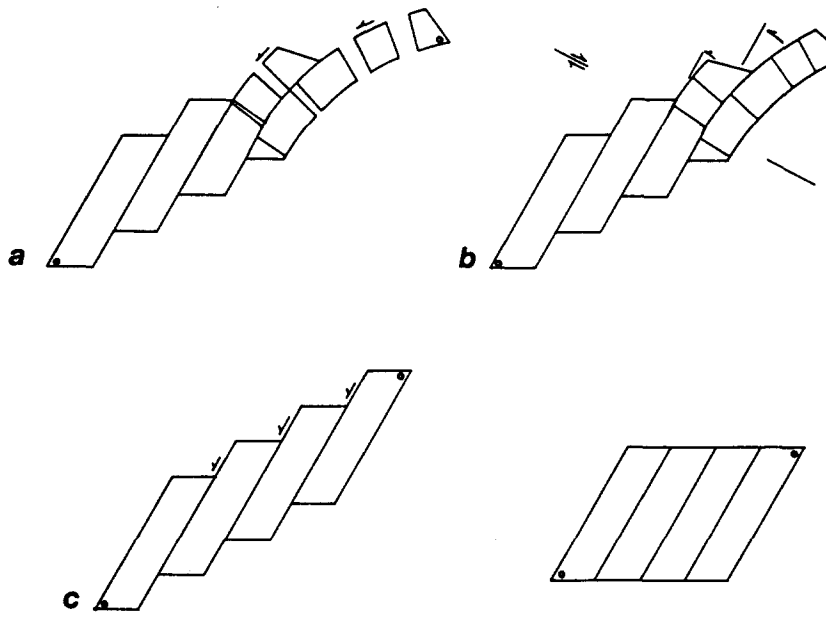


Fig. 7. Diagrams illustrating the reconstruction methods used to calculate strain values, dots as reference marks: (a) reassembly of microboudins to microfault blocks, (b) unbending of curved microfaults, line with shear arrows = axial plane of bend, (c) retrodeformation of normal microfaults.

Hylas zone at their southern terminations. The fold axis of the northernmost dome (Weems 1974) lies almost parallel to the Hylas zone. Dips are steeper on the eastern limbs (average 35–40°) than on the west (average 25–30°) indicating a slight asymmetry. Maximum domal uplift at the center of the State Farm dome (Fig. 2) is approximately 3.5 km using down-plunge projections. Farrar (1984) has identified other domes in the Maidens Gneiss to the west.

There are also many mesoscopic and small megascopic asymmetric folds in the area (Fig. 3) with consistent clockwise vergence. The folds appear intimately related to the large and small shear zones. Their consistency of vergence and orientation and close association with the shear zones indicates that they may be large-scale reverse-slip crenulations (Dennis & Secor 1987).

These meso- and megascopic strain features are consistent with the microstructural features. Although asymmetric fold vergence alone is not a reliable movement-sense indicator, the consistency of the clockwise rotation supports the dextral movement indicated by the microstructures. The mylonite in the Hylas zone was locally folded into similar clockwise verging asymmetric folds. The orientation and form of the domes is also characteristic of deformation associated with dextral transcurrent faulting. Harding & Lowell (1979) proposed that en échelon domes above a large strike-slip fault coalesced into positive flower structures in the Ardmore Basin, Oklahoma. The Goochland area domes probably formed in a similar manner. The domes formed with N–S fold axes that trace the long axis of the finite strain ellipsoid. The southern terminations of the domes were close enough to the Hylas zone to have been rotated into a northeast orientation during shearing. Gates (1987) identified similar structures along the Bowens Creek fault, a major dextral strike-slip shear zone in the southwestern Virginia Piedmont.

## TECTONO-THERMAL EVOLUTION

Many Ar–Ar and fission-track mineral dates have been determined on the rocks from the Hylas zone area (Bobyarchick & Glover 1979, Durrant 1979, Durrant *et al.* 1980). Together with zircon ages on the Petersburg granite (Wright *et al.* 1975) and peak $M_1$ metamorphic conditions, a thermal-decay or time–temperature curve has been constructed for the Alleghanian metamorphism (Fig. 8). The data analysis and methods of collection for this curve are presented in Durrant (1979). Excerpts of this work including sample locations, number of analyses and ages are presented in the Appendix. Because of uncertainties in ages and closure temperatures, the dates define a thermal-decay field rather than a curve. The distribution of ages of various minerals in the Goochland terrane shows no spatial trends. The terrane appears to have cooled relatively evenly, at least in the vicinity of the Hylas zone. The thermal-decay field is therefore generally applicable to the whole area.

To evaluate the timing of the mineral response to deformation, conditions of ductile response of quartz and feldspar are plotted on the thermal axis of the decay graph. Assuming geologically reasonable values for strain rate, hydroxyl contents of quartz, confining pressure and other parameters (see Watts & Williams 1979), feldspar is rigid to about 450 ± 50°C and quartz to about 300 ± 50°C (Sibson 1977, 1983, Tullis & Yund 1977). There may be a temperature difference in response between the feldspars.

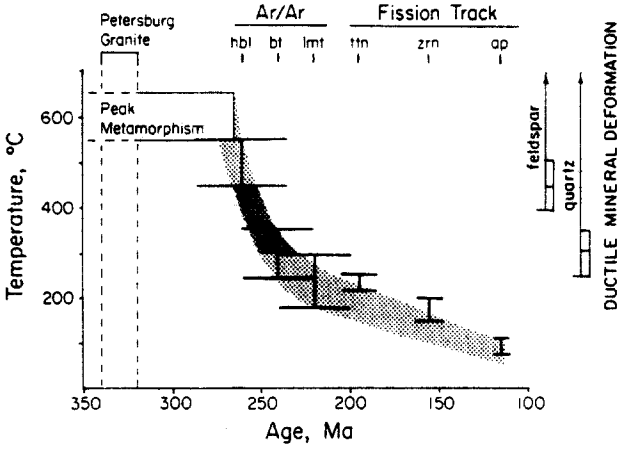


Fig. 8. Thermal-decay curve for Alleghanian metamorphism in the eastern Virginia Piedmont. Ar–Ar hornblende (hbl), and biotite (bt) and fission track titanite (ttn), apatite (ap) and zircon (zrn) ages from Durrant (1979), Ar–Ar laumontite (lmt) age from Bobyarchick (1976), U–Pb zircon ages from Wright *et al.* (1975) and peak metamorphic temperatures from Farrar (1984). Points include error bars both for time and temperature of closure. Temperature of brittle–ductile transition for feldspar and quartz from Tullis & Yund (1977) and Sibson (1977, 1983) and include uncertainty limits. See text for assumptions. Shaded path shows uncertainty; darker shade represents brittle–ductile transition.

The shortcomings in the application of mineral strain response to geochronologic thermal-decay curves for a terrane are not only geochronologic but also in temperature–mineral behavior correlations. The roles of feldspar composition, fluid composition and grain size in behavior are not well constrained with respect to temperature. The overprinting of the deformation types in the mylonite zone determine the order but their position on the decay curve may vary. In the Hylas zone, a shift of ±100°C would produce a ±20 Ma error in age because of the steepness of the curve. In terranes that were slowly uplifted and cooled, the errors may be more significant.

The development of *C* and *S* bands and rotated feldspar porphyroclasts in the Petersburg granite and shear bands with associated kyanite in the Maidens pelitic gneiss document ductile deformation at moderate to high temperature. The dynamic recrystallization of feldspars indicates temperatures in excess of 400°C (Tullis & Yund 1977) and the association metamorphic assemblages of kyanite + biotite + garnet with shear bands indicates peak $M_1$ metamorphic conditions of 550–650°C (Farrar 1984). The timing of the initiation of dextral transcurrent shearing in the Hylas zone is uncertain. Kyanite in the shear bands and the localization of the amphibolite-grade $M_1$ overprint along the Hylas zone (Farrar 1984) indicates that the dextral fault was active during $M_1$ metamorphism. The pre-kinematic 330 Ma Petersburg granite provides the best constraint to the initiation of shearing. Ar–Ar dating of hornblende yields a 262 Ma plateau age, the closure temperature of which is proposed to be 500 ± 50°C (Hanson & Gast 1971, Harrison & McDougall 1980). High-temperature ductile deformation probably continued to at least this time.

The later, lower temperature deformation was semi-brittle in nature. Quartz remained ductile exhibiting ribbon development whereas feldspar underwent brittle deformation. The temperature of deformation therefore ranged from 450 ± 50°C to 300 ± 50°C which is supported by the growth of metamorphic biotite, zoisite, albite and chlorite in the deformation zone. The brittle deformation may have post-dated that in the brittle–ductile transition, but could reflect elevated fluid pressure or an appropriate change in any of the other parameters that determine the brittle–ductile transition. The lower temperature shearing at the ductile–brittle transition occurred after 262 Ma (hornblende age) and ended before 241–221 Ma. Biotite yields an Ar–Ar age of 241 Ma which is proposed to represent cooling through 300 ± 50°C (Durrant *et al.* 1980). The 221 Ma Ar–Ar age on laumontite is difficult to evaluate but Bobyarchick (1976) suggested a closure temperature of approximately 250 ± 50°C based on mineral stability. The lower temperature portion of the curve is flatter than the early history. Deformation in this Mesozoic portion of the thermal decay curve was in the brittle regime. The dextral shearing apparently lasted into the Permian but bears an uncertain relation to Triassic rifting.

## CONCLUSIONS

The Hylas mylonite zone shows the same late Paleozoic dextral movement sense as the Nutbush Creek, Hollister and Modoc (Irmo) zones, the other major segments of the Eastern Piedmont fault systems. *S–C* mylonites in the Petersburg granite and kyanite bearing assemblages in ductile shear bands in the aluminous Maidens Gneiss indicate an early high-temperature ductile phase of deformation. Subsequent deformation at the brittle–ductile transition is indicated by ductile quartz ribbon development and a sequence of brittle feldspar textures that reflect strain intensity. Correlation of the mineral deformation responses to a thermal-decay curve based on isotopic mineral dating documents the timing of deformation. Dextral movement commenced subsequent to the intrusion of the 330 Ma Petersburg granite with deformation in the ductile regime. Deformation then crossed into the brittle–ductile transition at about 260 Ma and dextral transcurrent shearing probably terminated before about 240 Ma.

*Acknowledgements*—Field and laboratory work was funded through the Nuclear Regulatory Commission grant NRC 04-75-737 to Lynn Glover, III, and J. K. Costain. Thanks to Richard Gibson, Don Secor, Jr, John Sutter, an anonymous reviewer and especially to John Bartley for reviewing the manuscript. Thanks also to Jeff Durrant and John Sutter for allowing the publication of the isotopic data and C. Van Tyne for help with the SEM-EDS at Lafayette College.

## REFERENCES

Bartley, J. M., Turner, R. D., Mies, J., Druhan, R. & Butler, J. R. 1984. Kinematic analysis of the Nutbush Creek mylonite zone at

Satterwhite Point, Kerr Lake, North Carolina. *Geol. Soc. Am. Abs. w. Prog.* **15**, 124.

Berthé. D., Choukroune, P. & Jegouzo, P. 1979. Orthogneiss, mylonite and non-coaxial deformation of granites: the example of the South Amorican shear zone. *J. Struct. Geol.* **1**, 31–42.

Bobyarchick, A. R. 1976. Tectogenesis of the Hylas zone and eastern Piedmont near Richmond Virginia. Unpublished M.S. thesis, Virginia Polytechnic Institute and State University, Blacksburg, U.S.A.

Bobyarchick, A. R. 1981. The eastern Piedmont fault system and its relationship to Alleghanian tectonics in the southern Appalachians. *J. Geol.* **89**, 335–347.

Bobyarchick, A. R. & Glover, L., III. 1979. Deformation and metamorphism in the Hylas zone and adjacent parts of the eastern Piedmont in Virginia. *Bull. geol. Soc. Am.* **90**, 739–752.

Boullier, A. M. & Bouchez, J. -L. 1978. Le quartz en rubans dans les mylonites. *Bull. Soc. geol. Fr.* **20**, 253–262.

Bourland, W. C. 1976. Tectogenesis and metamorphism of the Piedmont from Columbia to Westview, Virginia along the James River. Unpublished M.S. thesis, Virginia Polytechnic Institute and State University, Blacksburg, U.S.A.

Dallmeyer, R. D., Wright, J. E., Secor, D. T., Jr. & Snoke, A. W. 1986. Character of the Alleghanian orogeny in the southern Appalachians: Part II. Geochronological constraints on the tectonothermal evolution of the eastern Piedmont in South Carolina. *Bull. geol. Soc. Am.* **97**, 1329–1344.

Debat, P., Soula, J. C., Kubin, L. & Vidal, J. L. 1978. Optical studies of natural deformation microstructures in feldspars (gneisses and pegmatites from Occitanie, southern France). *Lithos* **11**, 133–146.

Dennis, A. J. & Secor, D. T., Jr. 1987. A model for the development of crenulations in shear zones with applications from the Southern Appalachian Piedmont. *J. Struct. Geol.* **9**, 809–817.

Druhan, R. M. & Rollins, F. O. 1984. The Nutbush Creek fault zone in the Eastern Piedmont of North Carolina. *Geol. Soc. Am. Abs. w. Prog.* **16**, 135.

Durrant. J. M. 1979. Structural and metamorphic history of the Virginia Piedmont Province near Richmond, Virginia. Unpublished M.S. thesis, The Ohio State University, Columbus, U.S.A.

Durrant, J. M., Sutter, J. F. & Glover, L., III. 1980. Evidence for an Alleghanian (Hercynian?) metamorphic event in the Piedmont province near Richmond, Virginia. *Geol. Soc. Am. Abs. w. Prog.* **12**, 176.

Eisbacher, G. H. 1970. Deformation mechanics of mylonite rocks and fractured granulites in the Cobequid Mountains, Nova Scotia, Canada. *Bull. geol. Soc. Am.* **81**, 2009–2020.

Farrar, S. S. 1982. The Goochland granulite terrane, eastern Piedmont, Virginia: petrographic evidence of Grenville granulite facies and Alleghanian amphibolite facies metamorphism. *Geol. Soc. Am. Abs. w. Prog.* **14**, 17.

Farrar, S. S. 1984. The Goochland granulite terrane: remobilized Grenville basement in the eastern Virginia Piedmont. In: *The Grenville Event in the Appalachians and Related Topics* (edited by Bartholomew, M. J.). *Spec. Pap. geol. Soc. Am.* **194**, 215–227.

Gates, A. E. 1987. Transpressional dome formation in the southwestern Virginia Piedmont. *Am. J. Sci.* **287**, 927–949.

Gates, A. E., Simpson, C. & Glover, L., III. 1986. Appalachian Carboniferous dextral strike-slip faults: an example from Brookneal, Virginia. *Tectonics* **5**, 119–133.

Glover, L., III, Mose, D. G., Costain, J. K., Poland, F. B. & Reilly, J. M. 1982. Grenville basement in the Eastern Piedmont of Virginia: a progress report. *Geol. Soc. Am. Abs. w. Prog.* **14**, 20.

Glover, L., III, Mose, D. G., Poland, F. B., Bobyarchick, A. R. & Bourland, W. C. 1978. Grenville basement in the eastern Piedmont of Virginia: implications for orogenic models. *Geol. Soc. Am. Abs. w. Prog.* **10**, 169.

Glover, L., III, Speer, J. A., Russell, G. S. & Farrar, S. S. 1983. Ages of regional metamorphism and ductile deformation in the central and southern Appalachians. *Lithos* **16**, 223–245.

Hanson, G. N. & Gast, P. W. 1971. Kinetic studies in contact metamorphic zones. *Geochim. cosmochim. Acta* **35**, 101–107.

Harding, T. P. & Lowell, J. D. 1979. Structural styles, their plate tectonic habitats, and hydrocarbon traps in petroleum provinces. *Bull. Am. Ass. Petrol. Geol.* **63**, 1016–1058.

Harris, L. D., DeWitt, W. Jr. & Bayer, K. C. 1982. Interpretive seismic profile along I-64 from Valley and Ridge to the Coastal Plain in central Virginia. U.S. Geol. Surv. Oil Gas Inv. Chart OC-123.

Harrison, T. M. & McDougall, I. 1980. Investigations of an intrusive contact northwest Nelson, New Zealand: II. Diffusion of radiogenic and excess $^{40}Ar$ in hornblende revealed by $^{40}Ar/^{39}Ar$ age spectra analysis. *Geochim. cosmochim. Acta* **44**, 2005–2020.

Hatcher, R. D., Jr., Howell, D. E. & Talwani, P. 1977. Eastern Piedmont fault system: speculations on its extent. *Geology* **5**, 636–640.

Lister, G. S. & Snoke, A. W. 1984. S–C mylonites. *J. Struct. Geol.* **6**, 617–638.

Passchier, C. W. & Simpson, C. 1986. Porphyroclast systems as kinematic indicators. *J. Struct. Geol.* **8**, 831–843.

Platt, J. P. & Vissers, R. L. M. 1980. Extensional structures in anisotropic rocks. *J. Struct. Geol.* **2**. 397–410.

Poland, F. B. 1976. Geology of the rocks along the James River between Sabot and Cedar Point, Virginia. Unpublished M.S. thesis, Virginia Polytechnic Institute and State University, Blacksburg, U.S.A.

Pratt, T. L., Coruh, C., Costain, J. K. & Glover, L., III. 1988. A geophysical study of the earth's crust in central Virginia: implications for Appalachian crustal structure. *J. geophys. Res.* **93**, 6649–6667.

Reilly, J. M. 1980. A geologic and potential field investigation in the central Virginia Piedmont. Unpublished M.S. thesis, Virginia Polytechnic Institute and State University, Blacksburg, U.S.A.

Russell, G. S., Russell, C. W. & Farrar, S. S. 1985. Alleghanian deformation and metamorphism in the eastern North Carolina Piedmont. *Bull. geol. Soc. Am.* **96**. 381–387.

Secor, D. T., Jr., Snoke, A. W., Bramlett, K. W., Costello, O. P. & Kimbrill, O. P. 1986. Character of the Alleghanian orogeny in the southern Appalachians: Part I. Alleghanian deformation in the eastern Piedmont of South Carolina. *Bull. geol. Soc. Am.* **97**, 1319–1328.

Sibson, R. H. 1977. Fault rocks and fault mechanisms. *J. geol. Soc. Lond.* **133**, 190–213.

Sibson, R. H. 1983. Continental fault structure and the shallow earthquake source. *J. geol. Soc. Lond.* **140**, 741–767.

Simpson, C. 1985. Deformation of granitic rocks across the brittle–ductile transition. *J. Struct. Geol.* **7**. 503–511.

Simpson, C. 1986. Determination of movement sense in mylonites. *J. geol. Ed.* **34**. 246–261.

Simpson, C. & Schmid, S. M. 1983. An evaluation of criteria to deduce the sense of movement in sheared rocks. *Bull. geol. Soc. Am.* **94**, 1281–1288.

Smits, A. D., Stoddard, E. F. & Boltin, W. R. 1988. The Hollister mylonite zone in the North Carolina Piedmont. *Geol. Soc. Am. Abs. w. Prog.* **20**, 316.

Snoke, A. W. & Secor, D. T., Jr. 1983. The sense of shear in the Modoc zone, South Carolina Piedmont—implications for late Paleozoic geodynamic scenario. *Geol. Soc. Am. Abs. w. Prog.* **15**, 110.

Snoke, A. W., Kish, S. A. & Secor, D. T., Jr. 1980. Deformed Hercynian granitic rocks from the Piedmont of South Carolina. *Am. J. Sci.* **280**, 1018–1034.

Tullis, J. A. & Yund, R. A. 1977. Experimental deformation of dry Westerly Granite. *J. geophys. Res.* **82**, 5705–5718.

Tullis, J. A. & Yund, R. A. 1987. Transition from cataclastic flow to dislocation creep of feldspar: mechanisms and microstructures. *Geology* **15**, 591–686.

Watts, M. J. & Williams, G. D. 1979. Fault rocks as indicators of progressive shear deformation in the Guingamp region, Brittany. *J. Struct. Geol.* **1**, 323–332.

Weems, R. E. 1974. Geology of the Hanover Academy and Ashland quadrangles, Virginia. Unpublished M.S. thesis, Virginia Polytechnic Institute and State University, Blacksburg, U.S.A.

Williams, H. 1978. Tectonic lithofacies map of the Appalachian orogen, Map 1. Memorial University of Newfoundland, St. Johns.

Wright, J. E., Sinha, A. K. & Glover, L., III. 1975. Age of zircons from the Petersburg granite, Virginia: with comments on belts of plutons in the Piedmont. *Am. J. Sci.* **275**, 848–856.

## APPENDIX

$^{40}Ar$–$^{39}Ar$ weight average plateau ages (Ma) of samples from the Goochland terrane, eastern Piedmont, Virginia. Data from Durrant (1979), a M.S. thesis under the direction of John F. Sutter and available from the Ohio State University Geology Library upon request. Ages on thermal-decay curve are median averages from frequency distribution analyses. Sample locations on base map from Fig. 2. NP = no plateau

| | Sample | Age (Ma) |
|---|---|---|
| Biotite | | |
| | JDVP-14 | 337 ± 4 |
| | JDVP-19 | 243 ± 3 |
| | JDVP-23 | 230 ± 3 |
| | JDVP-26 (1) | 279 ± 3 |
| | JDVP-26 (2) | 284 ± 3 |
| | JDVP-28 | 234 ± 3 |
| | JD8-69 | 236 ± 3 |
| | JD8-78 | 254 ± 3 |
| | JD9-1A | 244 ± 3 |
| | JD9-3 | 230 ± 3 |
| | JD9-4 | 261 ± 4 |
| | JD9-6 | 235 ± 3 |
| | JD9-8 | 227 ± 3 |
| | JD9-9 | 226 ± 3 |
| | JD9-10 | 295 ± 4 |
| | JD9-12 (1) | 336 ± 3 |
| | JD9-12 (2) | 347 ± 4 |
| | JD9-14 | 271 ± 4 |
| | JD9-18 | 262 ± 3 |
| | JD9-20 | 272 ± 3 |
| | JD9-21 | 262 ± 3 |
| | JD9-23 | 241 ± 3 |
| Hornblende | | |
| | JDVP-23 | 244 ± 3 |
| | JDVP-27 | NP |
| | JD8-33 | 286 ± 4 |
| | JD8-71 | NP |
| | JD8-75 | NP |
| | JD8-79 | 256 ± 3 |
| | JD9-1B | 261 ± 3 |
| | JD9-4 | 276 ± 3 |
| | JD9-5 | NP |
| | JD9-12 | 264 ± 10 |
| | JD9-14 | 250 ± 3 |
| | JD9-22 | 270 ± 3 |
| | JD9-24 | 249 ± 3 |

Fission track ages (Ma) from the same source

| | Sample | Age (Ma) |
|---|---|---|
| Apatite | | |
| | JDVP-14 | 124 ± 12 |
| | JD9-4 | 123 ± 14 |
| | JD9-6 | 123 ± 14 |
| | JD9-10 | 111 ± 13 |
| | JD9-11 | 116 ± 13 |
| | JD9-14 | 120 ± 13 |
| | JD9-16 | 116 ± 14 |
| | JD9-18 | 108 ± 12 |
| Zircon | | |
| | JDVP-19 | 148 ± 15 |
| | JDVP-26 | 144 ± 14 |
| | JD9-16 | 161 ± 16 |
| | JD9-18 | 156 ± 16 |
| | JD9-20 | 171 ± 17 |
| | JD9-21 | 142 ± 14 |
| Titanite | | |
| | JD9-10 | 204 ± 20 |
| | JD9-14 | 183 ± 18 |

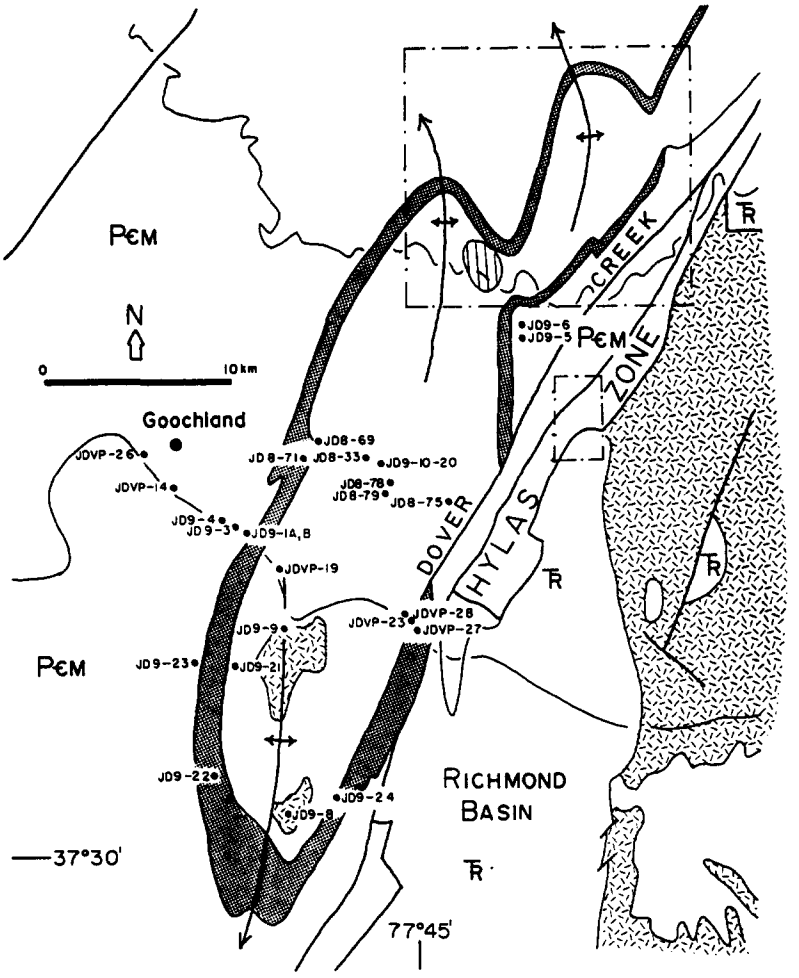


Fig. A1. Location map for $^{40}Ar$–$^{39}Ar$ and fission track samples. Geology from Fig. 2.